

UC Irvine

UC Irvine Previously Published Works

Title

Damped Topological Magnons in the Kagome-Lattice Ferromagnets

Permalink

<https://escholarship.org/uc/item/77d0r8vr>

Journal

Physical Review Letters, 117(18)

ISSN

0031-9007

Authors

Chernyshev, AL
Maksimov, PA

Publication Date

2016-10-28

DOI

10.1103/physrevlett.117.187203

Peer reviewed

Damped Topological Magnons in the Kagomé-Lattice Ferromagnets

A. L. Chernyshev¹ and P. A. Maksimov¹

¹*Department of Physics and Astronomy, University of California, Irvine, California 92697, USA*

(Dated: July 1, 2016)

We demonstrate that interactions can substantially undermine the free-particle description of magnons in ferromagnets on geometrically frustrated lattices. The anharmonic coupling, facilitated by the Dzyaloshinsky-Moria interaction, and a highly-degenerate two-magnon continuum yield a strong, non-perturbative damping of the high-energy magnon modes. We provide a detailed account of the effect for the $S=1/2$ ferromagnet on the kagomé lattice and propose further experiments.

PACS numbers: 75.10.Jm, 75.30.Ds, 75.40.Gb, 78.70.Nx

Theoretical proposals and experimental discoveries of electronic topological materials having bulk bands with nonzero topological invariants and protected edge states [1, 2] have lead to an active search for similar effects in systems with different quasiparticles [3–5]. Among the latter are magnon excitations in ferromagnets on frustrated lattices, with several materials identified, synthesized, and studied since the original proposal [5–9].

Simple Heisenberg ferromagnets have a classical, fully polarized ground state and their excitation spectra are affected by quantum effects only at a finite temperature [10], regardless of the underlying lattice. However, the lower symmetries of the geometrically-frustrated lattices, such as kagomé and pyrochlore, allow for a rather significant Dzyaloshinskii-Moriya (DM) interaction [8, 9]. While in their simplest form, the DM terms are frustrated, leaving the fully saturated ferromagnetic ground state intact, such a protection does not hold for the excited states. Instead, the DM interaction generates complex hopping amplitudes for the spin flips that translate into fluxes of fictitious fields, see Fig. 1(a), leading to Berry curvature of magnon bands. Among the consequences of this band transformation are unusual transport phenomena such as magnon Hall and spin Nernst effects [5–7, 11–14].

On closer inspection, the sought-after nontrivial topological character of magnon bands is intimately tied to several aspects of the underlying structures. In particular, their non-Bravais lattices necessarily host optical magnon branches, while the geometrically-frustrating lattice topology favors underconstrained couplings that result in the “flat” excitation branches featuring degeneracy points with the dispersive magnon bands, see Fig. 1(b). This degeneracy is lifted by the DM interaction, giving rise to the Berry curvature of the bands, which is responsible for nontrivial transport properties.

It has also been suggested that, in a minimal model, the topology of the bands can be “tuned” by manipulating the direction of magnetization [9, 14]. Using a small field to change the mutual orientation of magnetization \mathbf{M} and DM vector \mathbf{D} from $\mathbf{M} \parallel \mathbf{D}$ to $\mathbf{M} \perp \mathbf{D}$, one formally turns the DM-induced complex hoppings and the concomitant topological effects from “on” to “off” [9].

We point out that in all these constructions, an idealized, non-interacting free-boson description of magnons is simply taken for granted [11, 12, 15]. Below we demonstrate that such a free-quasiparticle picture of magnons in ferromagnets on the geometrically-frustrated lattices is missing a crucial physical effect, which, in turn, challenges conclusions reached within the idealized picture.

The key idea is that, for $\mathbf{M} \parallel \mathbf{D}$, the DM interaction is also a source of the anharmonic, particle-non-conserving coupling of magnons. The coupling is hidden for the ground state, but not for excitations, similarly to the complex hopping effect. Its most important outcome is a significant, non-perturbative damping of the flat and dispersive optical modes in the proximity of their degeneracy point, the effect precipitated by the divergent density of states in the two-magnon continuum. The resultant broadening at $\mathbf{k} \rightarrow 0$ is proportional to the first power of the DM term, $\Gamma \propto |\mathbf{D}|$, same as the band-splitting effect for $\mathbf{M} \parallel \mathbf{D}$. Interestingly, a sizable broadening has been noted as an unexpected result in a recent study of the kagomé-lattice ferromagnet, Cu(1-3,bdc), see Ref. [9].

Model and magnon interaction.—The nearest-neighbor model of a ferromagnet with the DM term is

$$\hat{\mathcal{H}} = -J \sum_{\langle ij \rangle} \mathbf{S}_i \cdot \mathbf{S}_j + \sum_{\langle ij \rangle} \mathbf{D}_{ij} \cdot (\mathbf{S}_i \times \mathbf{S}_j), \quad (1)$$

where $J > 0$, $\langle ij \rangle$ runs over bonds of the kagomé lattice, and Fig. 1(a) shows the order of i and j in the DM term, see [16]. While the DM interaction in the kagomé lat-

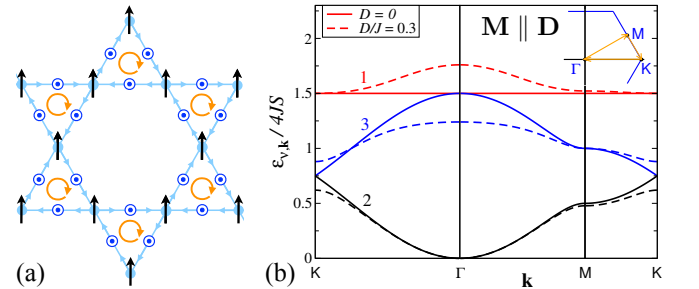


FIG. 1: (a) A ground state of (1) with $\mathbf{D}_{ij} = D\hat{\mathbf{z}}$; arrows on bonds show ordering of \mathbf{S}_i and \mathbf{S}_j in the DM term with fictitious fluxes indicated. (b) Magnon bands along the KΓMK path for $D=0$ (solid) and for $D/J=0.3$ with $\mathbf{M} \parallel \mathbf{D}$ (dashed).

tice can have both in- and out-of-plane components, the latter is dominant [17, 18]. In the following, we consider Hamiltonian (1) with $\mathbf{D}_{ij} = D\hat{\mathbf{z}}$ as a minimal model that illustrates a dramatic effect of magnon interactions.

Usually, the out-of-plane DM coupling would favor a canted in-plane order of spins with reduced magnetic moment due to quantum fluctuations in the ground state [19]. However, for ferromagnets on the geometrically-frustrated lattices it is the DM term that is frustrated. Thus, counterintuitively, magnetization remains fully saturated, $|\mathbf{M}| = SN$, regardless of its orientation with respect to \mathbf{D} . This is because the mean-field tug of the DM interactions on a given spin from its neighbors vanishes identically due to its cancellation from different bonds, see Fig. 1(a). For the same reason, the DM term cannot generate fluctuations in the saturated ground state. One can immediately see that the same is not true for magnon excitations, because spin flips violate cancellation of the DM contributions from different bonds. Therefore, while the ground state is insensitive to the DM interaction, the spectrum is not.

For the uniform out-of-plane \mathbf{D} , there are two principal directions for magnetization: $\mathbf{M} \parallel \mathbf{D}$ and $\mathbf{M} \perp \mathbf{D}$. The former case has been thoroughly examined within the linear spin-wave theory (LSWT) [5–9, 11–14] and we summarize it here briefly. Choosing the spin-quantization axis $\hat{\mathbf{z}} \parallel \mathbf{M} \parallel \mathbf{D}$ one can straightforwardly rewrite (1) as

$$\hat{\mathcal{H}} = -J \sum_{\langle ij \rangle} S_i^z S_j^z - \frac{1}{2} \sum_{\langle ij \rangle} (\mathcal{J} S_i^+ S_j^- + \mathcal{J}^* S_i^- S_j^+), \quad (2)$$

where $\mathcal{J} = J - iD$ and the DM term provides imaginary component to the spin-flip hoppings. Taking into account lattice geometry, rewriting spin flips as bosons, and diagonalizing the corresponding 3×3 matrix for the kagomé unit cell yields the harmonic-order, LSWT Hamiltonian

$$\hat{\mathcal{H}}^{(2)} = \sum_{\nu, \mathbf{k}} \varepsilon_{\nu, \mathbf{k}} b_{\nu, \mathbf{k}}^\dagger b_{\nu, \mathbf{k}}, \quad (3)$$

where the three magnon branches, $\varepsilon_{\nu, \mathbf{k}}$, are depicted in Fig. 1(b) for a representative value of D , see [16] for details. The main outcomes of the DM term are the gaps at the degeneracy points of the DM-free model, $\Delta \propto |\mathbf{D}|$, and the Berry curvature of the bands due to fictitious fields generated by complex hoppings [5, 12, 13]. It is clear that this procedure can be generalized to an *arbitrary* angle θ between \mathbf{M} and \mathbf{D} by simply replacing $D \rightarrow D \cos \theta$ in \mathcal{J} above. This immediately implies that for $\mathbf{M} \perp \mathbf{D}$ the complex hoppings cease completely and magnon bands should become free of the DM interaction, i.e., equivalent to the $D=0$ picture in Fig. 1(b).

A flaw in this reasoning is in the harmonic approximation. Although for $\mathbf{M} \perp \mathbf{D}$ the DM interaction does not contribute to the LSWT, it *does not* disappear. For the quantization axis $\hat{\mathbf{z}} \parallel \mathbf{M} \perp \mathbf{D}$, the DM term becomes

$$\hat{\mathcal{H}}_{DM} = \frac{D}{2} \sum_{\langle ij \rangle} [(S_i^+ + S_i^-) S_j^z - S_i^z (S_j^+ + S_j^-)], \quad (4)$$

which indeed does not affect the ground state or harmonic theory. However, it gives rise to anharmonic interaction of magnons [20] as it creates/annihilates a spin-flip in a proximity of another spin flip, with contributions from the nearest bonds not canceling out. Thus, transitions are generated between single- and two-magnon states, which can lead to renormalization of the bands and, most importantly, to magnon damping.

With the formal details given in [16], the resultant cubic interaction of magnons obtained from (4) is [21]

$$\hat{\mathcal{H}}_{DM}^{(3)} = \frac{D}{2!} \sqrt{\frac{2S}{N}} \sum_{\mathbf{k}, \mathbf{q}} \sum_{\nu\mu\eta} \tilde{\Phi}_{\mathbf{q}\mathbf{k};\mathbf{p}}^{\nu\mu\eta} b_{\nu, \mathbf{q}}^\dagger b_{\mu, \mathbf{k}}^\dagger b_{\eta, \mathbf{p}} + \text{H.c.}, \quad (5)$$

with the vertex $\tilde{\Phi}_{\mathbf{q}\mathbf{k};\mathbf{p}}^{\nu\mu\eta} = F_{\mathbf{q}\mathbf{k}\mathbf{p}}^{\nu\mu\eta} + F_{\mathbf{k}\mathbf{q}\mathbf{p}}^{\mu\nu\eta}$ and the amplitude

$$F_{\mathbf{q}\mathbf{k}\mathbf{p}}^{\nu\mu\eta} = \sum_{\alpha\beta} \varepsilon^{\alpha\beta\gamma} \cos(q\beta\alpha) w_{\nu, \alpha}(\mathbf{q}) w_{\mu, \beta}(\mathbf{k}) w_{\eta, \beta}(\mathbf{p}), \quad (6)$$

where $\mathbf{w}_\nu = (w_{\nu,1}, w_{\nu,2}, w_{\nu,3})$ are the eigenvectors of the 3×3 matrix diagonalized for the harmonic theory. A generalization of this consideration to an arbitrary \mathbf{M} - \mathbf{D} angle is achieved by $D \rightarrow D \sin \theta$ in (4) and (5), also keeping in mind that the eigenvectors \mathbf{w}_ν in (6) change with $D \cos \theta$ according to the diagonalization leading to (3). Thus, the harmonic and the anharmonic Hamiltonians (3) and (5) complement each other for any $\theta \neq 0$.

We note that at $T=0$, the four-magnon terms do not directly affect the spectrum of the model (1) as they necessarily have a $b^\dagger b^\dagger b b$ form [16, 22].

Kinematics and two-magnon DoS.—Because the anharmonic term (5) provides a coupling of the single-particle branches with the two-magnon continuum, the properties of the latter are of interest. Consider $\mathbf{M} \perp \mathbf{D}$. From the point of view of the harmonic theory, magnon bands are not affected by the DM term, see Fig. 2, with the flat band (mode 1) degenerate with the dispersive band (mode 3) at the Γ point. Crucially, the two-magnon continuum is highly degenerate at this point because of a ubiquitous property of the magnon spectra of ferromagnets on the non-Bravais lattices. Namely, the two dispersive modes are mirror reflections of each other with

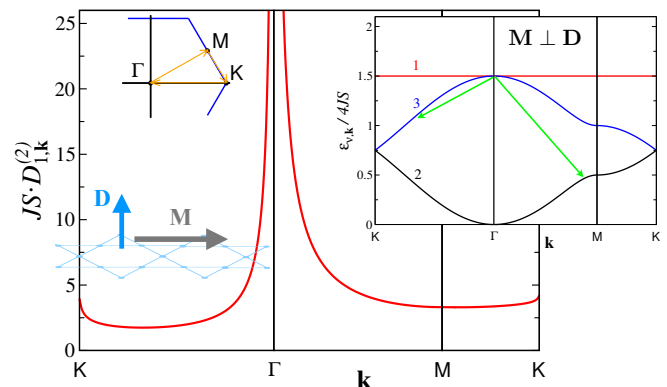


FIG. 2: The LSWT two-magnon DoS (7) for mode 1, $\mathbf{M} \perp \mathbf{D}$. Inset: schematics of a magnon decay from $\mathbf{k}=0$.

respect to their energy at the K-point, which is also precisely one half of the flat mode energy, see Fig. 2. One can easily check that the same structure persists for the pyrochlore and honeycomb lattices [8, 23, 24]. Because of that property, the condition $\varepsilon_1 = \varepsilon_{2,\mathbf{q}} + \varepsilon_{3,-\mathbf{q}}$ is met for *any* value of the momentum \mathbf{q} . This is a much higher degeneracy than the ones leading to more traditional van Hove singularities of the two-magnon continua [20].

A useful quantitative characteristics of the continuum is the on-shell, $\omega = \varepsilon_{\mu,\mathbf{k}}$, two-magnon density-of-states (DoS), which is also a proxy of the on-shell decay rate

$$D_{\mu,\mathbf{k}}^{(2)} = \pi \sum_{\mathbf{q},\nu\eta} \delta(\varepsilon_{\mu,\mathbf{k}} - \varepsilon_{\nu,\mathbf{q}} - \varepsilon_{\eta,\mathbf{k}-\mathbf{q}}), \quad (7)$$

shown in Fig. 2 for the flat mode, $\mu=1$, vs \mathbf{k} . It exhibits a strong $1/|\mathbf{k}|$ divergence at $\mathbf{k} \rightarrow 0$ due to the high degeneracy in the two-magnon continuum discussed above. The divergent behavior at $\mathbf{k} \rightarrow 0$ is identical for $\mu=3$ [16].

This consideration implies that an *arbitrary weak* coupling of the single-magnon and two-magnon states completely invalidates predictions of the harmonic theory by causing a divergent damping in the optical magnons at $\mathbf{k} \rightarrow 0$. As is shown below, a self-consistent treatment regularizes this divergence, but leaves an anomalously large, non-analytic and non-perturbative damping, $\Gamma \propto |\mathbf{D}|$, for both optical magnon modes near the Γ -point and in a broad range of $|\mathbf{k}| \lesssim D/J$ also controlled by D .

Decays and regularization.—One can expect the on-shell decay rate of a magnon due to cubic terms (5)

$$\Gamma_{\mu,\mathbf{k}} = \frac{\pi S D^2}{N} \sum_{\mathbf{q},\nu\eta} |\tilde{\Phi}_{\mathbf{q},\mathbf{k}-\mathbf{q};\mathbf{k}}^{\nu\eta\mu}|^2 \delta(\varepsilon_{\mu,\mathbf{k}} - \varepsilon_{\nu,\mathbf{q}} - \varepsilon_{\eta,\mathbf{k}-\mathbf{q}}), \quad (8)$$

to be small for realistic parameters as it is $\propto D^2/J$. This is indeed the case for the Goldstone branch (mode 2), for which damping is also suppressed kinematically except for large momenta [16]. However, because of the degeneracy of the two-magnon DoS, damping (8) of the mode 3 is divergent as $1/|\mathbf{k}|$, thus suggesting a much stronger effect. The situation is less conspicuous for the flat mode, as the expected similar divergence in (8) is preempted by a subtle cancellation in the vertex, leading to a finite, $O(D^2)$, damping at $\mathbf{k} \rightarrow 0$ [16]. However, this cancellation is lifted in the off-shell consideration, which, counterintuitively, leads to a strongly enhanced decay rate of the flat mode in the self-consistent treatment. We note that the real part of the same self-energy [25] also diverges for both optical magnon modes, but its divergence is much weaker [16], $\text{Re} \Sigma_{\mu,\mathbf{k}} \propto \ln |\mathbf{k}|$.

A regularization of the divergencies is achieved via a self-consistent solution of the Dyson's equation (DE), which naturally accounts for the damping of the initial-state magnon, $\omega - \varepsilon_{\mu,\mathbf{k}} - \Sigma_{\mu,\mathbf{k}}(\omega^*) = 0$, where $\Sigma_{\mu,\mathbf{k}}(\omega)$ is the self-energy due to cubic terms and the complex conjugate ω^* respects causality, see [26]. The real and imaginary parts of this equation have to be solved together. However, once the initial-state damping is introduced, the weak divergence in the real part will be

cut [26]. Therefore, for small $d=D/J$, it will constitute a small energy correction, $\propto d^2 \ln |d|$, neglecting which yields an “imaginary-only” Dyson's equation, which we coin as iDE: $\Gamma_{\mu,\mathbf{k}} = -\text{Im} \Sigma_{\mu,\mathbf{k}}(\varepsilon_{\mu,\mathbf{k}} + i\Gamma_{\mu,\mathbf{k}})$, or, explicitly

$$1 = \frac{S D^2}{N} \sum_{\mathbf{q},\nu\eta} \frac{|\tilde{\Phi}_{\mathbf{q},\mathbf{k}-\mathbf{q};\mathbf{k}}^{\nu\eta\mu}|^2}{(\varepsilon_{\mu,\mathbf{k}} - \varepsilon_{\nu,\mathbf{q}} - \varepsilon_{\eta,\mathbf{k}-\mathbf{q}})^2 + \Gamma_{\mu,\mathbf{k}}^2}. \quad (9)$$

With the numerical results for the iDE to follow, its key result can be appreciated. At small $|\mathbf{k}|$, the difference of magnon energies in (9) for the divergent decay channels $\mu \rightarrow \{2, 3\}$ is negligible, giving: $\Gamma_{\mu,\mathbf{k} \rightarrow 0} \approx |D| \sqrt{S}$. Physically, the “fuzziness” of the initial-state magnon removes strict energy-momentum conservations in the decay process, regularizing the divergencies.

This constitutes the main result of the iDE regularization. The decay rate of both flat and gapped modes for $\mathbf{M} \perp \mathbf{D}$ at $\mathbf{k} \rightarrow 0$ is given by a non-perturbative answer, $\Gamma_{1(3),\mathbf{k}} \propto |D|$, strongly enhanced compared to the perturbative expectations. The \mathbf{k} -region in which the broadening is strongly enhanced can be easily estimated as $|\mathbf{k}| \lesssim |\mathbf{k}^*| \propto |D|/J$ with the damping decreasing to the perturbative values, $\Gamma_{3(1),\mathbf{k}} \propto D^2/J$, for $|\mathbf{k}| \gtrsim |\mathbf{k}^*|$.

The numerical solutions of the iDE (9) for damping $\Gamma_{\mathbf{k}}$ for all three magnon modes for $S=1/2$ and $D/J=0.3$ are shown in Fig. 3 along the K Γ MK path. One can see that, indeed, the damping is strongly enhanced in the $|\mathbf{k}| \lesssim |D|/J$ region around the Γ point for the flat and dispersive optical modes, see also [16] for other values of D/J . The inset shows the full width of magnon spectral lines at half-maximum, $\varepsilon_{\mathbf{k}} \pm \Gamma_{\mathbf{k}}$, to demonstrate effects of the broadening on the magnon spectrum. One can also see that the decay rates of modes 1 and 3 at $\mathbf{k}=0$ coincide because of the symmetry of the the cubic vertices [16]. Some remnants of the more conventional, logarithmic van Hove singularities [20] can be seen in both Figs. 3 and 4.

Angular dependence.—Since magnetization is not pinned for model (1), one can manipulate its direction. Then, the natural question is: how does one transition from the well-defined excitations with the gap $\propto D$ to the broadened excitations with the widths $\propto D$ as a function of the \mathbf{M} - \mathbf{D} angle θ ?

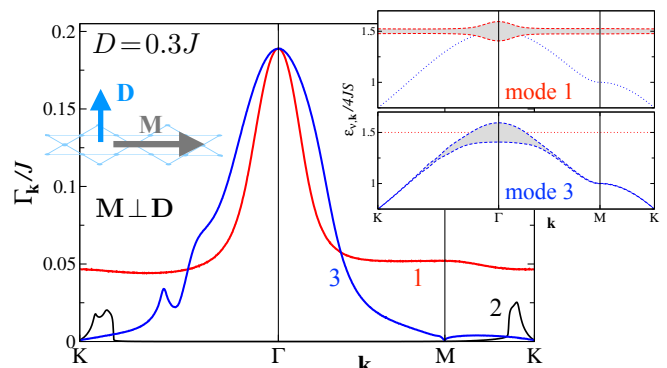


FIG. 3: Solutions of the iDE (9) for $D/J=0.3$, $S=1/2$ along the K Γ MK path. Inset: the FWHM of spectral lines, $\varepsilon_{\mathbf{k}} \pm \Gamma_{\mathbf{k}}$.

For $\theta < \pi/2$, magnetization is partially along \mathbf{D} and magnon bands split due to complex hoppings ($\sim \cos\theta$), while cubic interaction in (5) is reduced ($\sim \sin\theta$) as described above. The main complication is that, for $\mathbf{M} \not\perp \mathbf{D}$, the eigenvectors in the vertices (6), \mathbf{w}_ν , are not derivable analytically in a compact form [27], and have to be obtained numerically from diagonalization of the 3×3 matrix [16]. Physically, the band splitting also contributes to regularization of singularities in magnon decays.

In Fig. 4, we provide detailed predictions for the angular dependence of the damping of the optical magnon modes obtained from iDE (9). Fig. 4(a) shows a gradual decrease of the broadening for both modes at $\mathbf{k}=0$ from its maximal value to zero upon the decrease of the angle θ , with the insets showing $\Gamma_{\mu,\mathbf{k}}$ along the KFM path for several values of the angle. Fig. 4(b) panels present the 2D intensity plots of the broadening of the mode 3 in \mathbf{k} -space for three different angles. These results complement the data in Figs. 3 and 4(a) and demonstrate a rather dramatic distribution of the broadening in the Brillouin zone and its nontrivial evolution with the angle. This detailed picture is completed in Fig. 4(c) by the $\mathbf{k} - \theta$ intensity maps of the broadening for both optical modes along the KFM path. They reveal an interesting contribution of the conventional van Hove singularities of the two-magnon continuum and highlight an unusual evolution of the magnon linewidth.

Our minimal-model consideration may seem to imply that there is always a special direction of \mathbf{M} that can allow one to switch off cubic anharmonic coupling and associated decay effects. However, in a more general and realistic setting, the DM term has both in- and out-of-plane components [8, 9], making magnon decays inevitable. It is, thus, imperative to take their effects into account in a consideration of magnon bands in real materials.

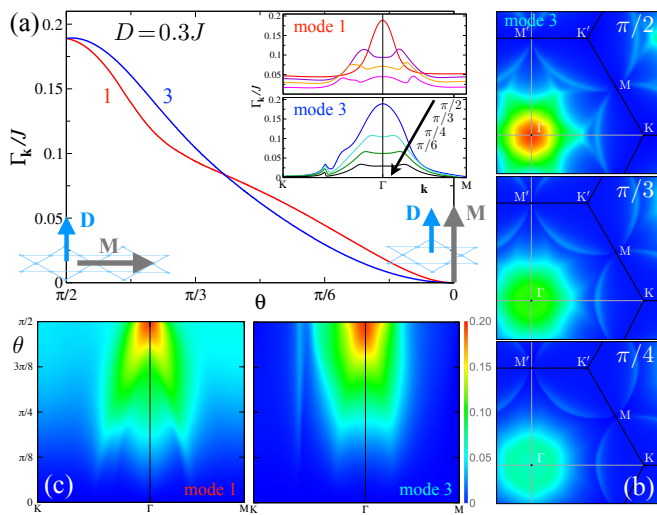


FIG. 4: (a) $\Gamma_{1(3),\mathbf{k}=0}$ vs θ . Insets: $\Gamma_{\mu,\mathbf{k}}$ along the KFM path for several θ . (b) The 2D intensity distributions of $\Gamma_{3,\mathbf{k}}$ in \mathbf{k} -space for $\pi/2$, $\pi/3$, and $\pi/4$. (c) The $\mathbf{k} - \theta$ intensity maps of $\Gamma_{1(3),\mathbf{k}}$ along the KFM path. $D/J=0.3$, $S=1/2$.

Experiments.—Experimental evidence of the broadening of the flat mode in the vicinity of $\mathbf{k} = 0$ has been recently reported for a kagome-lattice ferromagnet with $D_z/J \approx 0.15$ [9]. For $\mathbf{M} \perp \mathbf{D}$, the broadening varying from $0.05J$ in external field to $0.13J$ in zero field was suggested, see Supplemental material of [9]. Our consideration yields the broadening of both optical modes of a somewhat lesser value of $0.09J$ in zero field [16]. One can suggest that a larger broadening can be registered due to the overlap of the two modes. Other experimental factors that can affect a direct comparison include averaging of the data over a range of \mathbf{k} and contributions of the in-plane DM components to decays. The close agreement with the available data and our detailed predictions above call for a closer experimental analysis of the suggested dramatic broadening effects. They can be tested by the neutron-scattering, resonant neutron-scattering spin-echo, and by ESR.

Summary.—We demonstrated that the idea of non-interacting topologically nontrivial bands, familiar from fermionic systems, cannot be trivially transplanted to bosonic systems such as ferromagnets on the geometrically frustrated lattices. The key difference is in the particle-non-conserving terms that are generated by the same interactions that are necessary for the sought-after Berry curvature of the bands. These terms, combined with a ubiquitous degeneracy of the two-magnon continuum, produce a substantial broadening of magnon bands precisely in the ranges of \mathbf{k} and ω that are essential for the topological properties to occur, thus potentially undermining the entire free-band consideration. How the topologically-nontrivial properties of the bands can be defined in the presence of a substantial broadening remains an open question.

Acknowledgments.—We acknowledge useful conversations with Sid Parameswaran and Dima Pesin. A. L. C. is particularly indebted to Mike Zhitomirsky for an enlightening discussion on the kagome-lattice ferromagnetic state and cubic terms and to Oleg Starykh for his persistence in attracting our interest to the spectral properties of these systems, numerous conversations, and important comments. This work was supported by the U.S. Department of Energy, Office of Science, Basic Energy Sciences under Award # DE-FG02-04ER46174. A. L. C. would like to thank the Kavli Institute for Theoretical Physics where this work was initiated. The work at KITP was supported in part by NSF Grant No. NSF PHY11-25915.

- [1] M. Z. Hasan and C. L. Kane, Rev. Mod. Phys. **82**, 3045 (2010).
- [2] M. Z. Hasan and J. E. Moore, Annual Review of Condensed Matter Physics **2**, 55 (2011).
- [3] S. A. Parameswaran, I. Kimchi, A. M. Turner, D. M. Stamper-Kurn, and A. Vishwanath, Phys. Rev. Lett. **110**, 125301 (2013).

- [4] O. Hosten and P. Kwiat, *Science* **319**, 787 (2008); L. Zhang, J. Ren, J.-S. Wang, and B. Li, *Phys. Rev. Lett.* **105**, 225901 (2010).
- [5] H. Katsura, N. Nagaosa, and P. A. Lee, *Phys. Rev. Lett.* **104**, 066403 (2010).
- [6] T. Ideue, Y. Onose, H. Katsura, Y. Shiomi, S. Ishiwata, N. Nagaosa, and Y. Tokura, *Phys. Rev. B* **85**, 134411 (2012).
- [7] M. Hirschberger, R. Chisnell, Y. S. Lee, and N. P. Ong, *Phys. Rev. Lett.* **115**, 106603 (2015).
- [8] M. Mena, R. S. Perry, T. G. Perring, M. D. Le, S. Guerrero, M. Storni, D. T. Adroja, C. Rüegg, and D. F. McMorrow, *Phys. Rev. Lett.* **113**, 047202 (2014).
- [9] R. Chisnell, J. S. Helton, D. E. Freedman, D. K. Singh, R. I. Bewley, D. G. Nocera, and Y. S. Lee, *Phys. Rev. Lett.* **115**, 147201 (2015).
- [10] F. J. Dyson, *Phys. Rev.* **102**, 1230 (1956).
- [11] L. Zhang, J. Ren, J.-S. Wang, and B. Li, *Phys. Rev. B* **87**, 144101 (2013).
- [12] A. Mook, J. Henk, and I. Mertig, *Phys. Rev. B* **89**, 134409 (2014).
- [13] E. G. Mishchenko and O. A. Starykh, *Phys. Rev. B* **90**, 035114 (2014).
- [14] A. A. Kovalev and V. Zyuzin, *Phys. Rev. B* **93**, 161106 (2016).
- [15] R. Matsumoto, R. Shindou, and S. Murakami, *Phys. Rev. B* **89**, 054420 (2014).
- [16] See Supplemental Material at <http://link.aps.org/supplemental/>, for details on the non-linear spin-wave theory, solution of the self-consistent Dyson equation, and results for the other values of D/J .
- [17] M. Elhajal, B. Canals, and C. Lacroix, *Phys. Rev. B* **66**, 014422 (2002).
- [18] O. Cepas, C. M. Fong, P. W. Leung, and C. Lhuillier, *Phys. Rev. B* **78**, 140405 (2008).
- [19] T. Nikuni and A. E. Jacobs, *Phys. Rev. B* **57**, 5205 (1998); A. L. Chernyshev, *Phys. Rev. B* **72**, 174414 (2005); M. Janoschek, F. Bernlochner, S. Dunsiger, C. Pfleiderer, P. Böni, B. Roessli, P. Link, and A. Rosch, *Phys. Rev. B* **81**, 214436 (2010).
- [20] M. E. Zhitomirsky and A. L. Chernyshev, *Rev. Mod. Phys.* **85**, 219 (2013).
- [21] A. L. Chernyshev and M. E. Zhitomirsky, *Phys. Rev. Lett.* **113**, 237202 (2014); *Phys. Rev. B* **92**, 144415 (2015).
- [22] The higher- n -magnon terms have a similar structure, $(b^\dagger)^m (b)^{m'}$, with $m + m' = n$ and $m, m' \geq 2$.
- [23] P. A. Maksimov and A. L. Chernyshev, *Phys. Rev. B* **93**, 014418 (2016).
- [24] This is due to tight-binding form of magnon bands [16].
- [25] We neglect the off-diagonal terms in the self-energy as their contributions to the spectrum are of higher order, $O(d^4)$ in the Born approximation, see also [16].
- [26] A. L. Chernyshev and M. E. Zhitomirsky, *Phys. Rev. B* **79**, 144416 (2009).
- [27] See [5] (Supplemental) for analytical solution. Since our self-consistent procedure is already numerical, we perform the diagonalization numerically.

Damped Topological Magnons in the Kagomé-Lattice Ferromagnets: Supplemental Material

A. L. Chernyshev¹ and P. A. Maksimov¹

¹*Department of Physics and Astronomy, University of California, Irvine, California 92697, USA*

(Dated: June 29, 2016)

The formalism of the spin-wave theory is similar to the antiferromagnetic case [1] in several technical aspects. We present them here for completeness.

Heisenberg term, unit cell, etc.

The nearest-neighbor Heisenberg Hamiltonian reads

$$\hat{\mathcal{H}} = -J \sum_{\langle ij \rangle} \mathbf{S}_i \cdot \mathbf{S}_j, \quad (\text{S1})$$

where summation is over bonds, i and j are the sites of the kagomé lattice, $J > 0$. The unit cell can be chosen as an up triangle with three atoms at

$$\boldsymbol{\rho}_1 = (0, 0), \quad \boldsymbol{\rho}_2 = \left(-\frac{1}{4}, \frac{\sqrt{3}}{4}\right), \quad \boldsymbol{\rho}_3 = \left(-\frac{1}{2}, 0\right). \quad (\text{S2})$$

The distances are in units of $2a$ with a being the interatomic distance. The Bravais lattice is a triangular lattice with the primitive vectors

$$\boldsymbol{\delta}_1 = (1, 0), \quad \boldsymbol{\delta}_2 = \left(\frac{1}{2}, \frac{\sqrt{3}}{2}\right), \quad \boldsymbol{\delta}_3 = \boldsymbol{\delta}_2 - \boldsymbol{\delta}_1, \quad (\text{S3})$$

such that $\boldsymbol{\rho}_2 = \frac{1}{2}\boldsymbol{\delta}_3$ and $\boldsymbol{\rho}_3 = -\frac{1}{2}\boldsymbol{\delta}_1$, see Fig. 1. Changing the lattice sum to the sum over the unit cells ℓ and atomic index $\alpha = 1, 2, 3$, Hamiltonian (S1) becomes

$$\begin{aligned} \hat{\mathcal{H}} = & -J \sum_{\ell} \mathbf{S}_{1,\ell} \cdot (\mathbf{S}_{2,\ell} + \mathbf{S}_{2,\ell-3}) \\ & + \mathbf{S}_{1,\ell} \cdot (\mathbf{S}_{3,\ell} + \mathbf{S}_{3,\ell+1}) + \mathbf{S}_{2,\ell} \cdot (\mathbf{S}_{3,\ell} + \mathbf{S}_{3,\ell+2}), \end{aligned} \quad (\text{S4})$$

where $\ell \pm n \equiv \mathbf{R}_{\ell} \pm \boldsymbol{\delta}_n$ with the coordinate of the unit cell $\mathbf{R}_{\ell} = m_1\boldsymbol{\delta}_1 + m_2\boldsymbol{\delta}_2$.

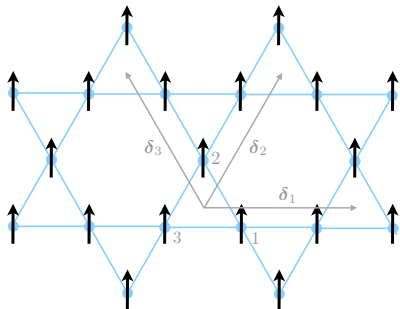


FIG. 1: Ferromagnetic state and numeration of sites within the unit cell with the primitive vectors of the kagomé lattice.

Linear spin-wave theory

Choosing the quantization axis in any direction and keeping only quadratic terms from the Holstein-Primakoff representation for spins in (S4), the harmonic Hamiltonian for bosonic magnon operators, $a_{\alpha,\ell}(a_{\alpha,\ell}^\dagger)$, is

$$\begin{aligned} \hat{\mathcal{H}}^{(2)} = & 4JS \sum_{\ell} \left\{ \left[a_{1,\ell}^\dagger a_{1,\ell} + a_{2,\ell}^\dagger a_{2,\ell} + a_{3,\ell}^\dagger a_{3,\ell} \right] \right. \\ & - \frac{1}{4} \left[a_{1,\ell}^\dagger (a_{2,\ell} + a_{2,\ell-3}) + a_{1,\ell}^\dagger (a_{3,\ell} + a_{3,\ell+1}) \right. \\ & \left. \left. + a_{2,\ell}^\dagger (a_{3,\ell} + a_{3,\ell+2}) + \text{H.c.} \right] \right\}. \end{aligned} \quad (\text{S5})$$

Performing Fourier transformation according to

$$a_{\alpha,\ell} = \frac{1}{\sqrt{N}} \sum_{\mathbf{k}} a_{\alpha,\mathbf{k}} e^{i\mathbf{k}\mathbf{r}_{\alpha,\ell}} \quad (\text{S6})$$

where $\mathbf{r}_{\alpha,\ell} = \boldsymbol{\rho}_\alpha + \mathbf{R}_\ell$ and N is the number of unit cells, we obtain the harmonic Hamiltonian

$$\hat{\mathcal{H}}^{(2)} = 4JS \sum_{\mathbf{k},\alpha\beta} \left(\delta_{\alpha\beta} - \frac{1}{2} \Lambda_{\mathbf{k}}^{\alpha\beta} \right) a_{\alpha,\mathbf{k}}^\dagger a_{\beta,\mathbf{k}}, \quad (\text{S7})$$

where we use the (traceless) matrix

$$\hat{\Lambda}_{\mathbf{k}} = \begin{pmatrix} 0 & c_3 & c_1 \\ c_3 & 0 & c_2 \\ c_1 & c_2 & 0 \end{pmatrix}, \quad (\text{S8})$$

with $c_n = \cos(q_n)$ and $q_n = \mathbf{k} \cdot \boldsymbol{\delta}_n/2$.

One can rewrite this Hamiltonian in the matrix form

$$\hat{\mathcal{H}}^{(2)} = \sum_{\mathbf{k}>0} \hat{X}_{\mathbf{k}}^\dagger \hat{\mathbf{H}}_{\mathbf{k}} \hat{X}_{\mathbf{k}} - 6JSN, \quad (\text{S9})$$

with the vector operator

$$\hat{X}_{\mathbf{k}}^\dagger = (a_{1,\mathbf{k}}^\dagger, a_{2,\mathbf{k}}^\dagger, a_{3,\mathbf{k}}^\dagger, a_{1,-\mathbf{k}}, a_{2,-\mathbf{k}}, a_{3,-\mathbf{k}}) \quad (\text{S10})$$

and the 6×6 matrix $\hat{\mathbf{H}}_{\mathbf{k}}$

$$\hat{\mathbf{H}}_{\mathbf{k}} = 4JS \begin{pmatrix} \hat{\mathbf{A}}_{\mathbf{k}} & \mathbf{0} \\ \mathbf{0} & \hat{\mathbf{A}}_{\mathbf{k}} \end{pmatrix}, \quad \hat{\mathbf{A}}_{\mathbf{k}} = \hat{\mathbf{I}} - \frac{1}{2} \hat{\Lambda}_{\mathbf{k}}, \quad (\text{S11})$$

where $\hat{\mathbf{I}}$ is the identity matrix.

Thus, the eigenvalues of $\hat{\mathbf{H}}_{\mathbf{k}}$ and $\hat{\mathbf{A}}_{\mathbf{k}}$ are straightforwardly related to the eigenvalues of the matrix $\hat{\Lambda}_{\mathbf{k}}$, so that the spin-wave excitation energies are

$$\varepsilon_{\nu,\mathbf{k}} = 4JS\omega_{\nu,\mathbf{k}} = 4JS(1 - \lambda_{\nu,\mathbf{k}}/2). \quad (\text{S12})$$

We note that because the nearest-neighbor magnon hoppings connect only different sublattices, $\text{tr}(\hat{\Lambda}_{\mathbf{k}}) = \sum_{\nu} \lambda_{\nu, \mathbf{k}} = 0$. This leads to an important property, common to the other non-Bravais lattices, such as pyrochlore and honeycomb. Namely, $\sum_{\nu} \varepsilon_{\nu, \mathbf{k}} = \text{const.}$

The characteristic equation for the matrix $\hat{\Lambda}_{\mathbf{k}}$ is

$$|\hat{\Lambda}_{\mathbf{k}} - \lambda| = (\lambda + 1)(\lambda^2 - \lambda - 2\gamma_{\mathbf{k}}) = 0, \quad (\text{S13})$$

where $\gamma_{\mathbf{k}} \equiv c_1 c_2 c_3$ and factorization is performed with the help of an identity $c_1^2 + c_2^2 + c_3^2 = 1 + 2c_1 c_2 c_3$. Thus, the λ -eigenvalues are

$$\lambda_1 = -1, \quad \lambda_{2(3), \mathbf{k}} = \frac{1}{2} \left(1 \pm \sqrt{1 + 8\gamma_{\mathbf{k}}} \right), \quad (\text{S14})$$

and the spin-wave energies are

$$\varepsilon_{1, \mathbf{k}} = 6JS, \quad \varepsilon_{2(3), \mathbf{k}} = JS(3 \mp \sqrt{1 + 8\gamma_{\mathbf{k}}}). \quad (\text{S15})$$

where one of the spin-wave excitations, $\varepsilon_{1, \mathbf{k}}$, is completely dispersionless (“flat mode”) and it is at the highest energy. The lowest energy mode, $\varepsilon_{2, \mathbf{k}}$, (Godstone branch) has a \mathbf{k}^2 dispersion near the Γ point as to be expected in a ferromagnet. All three modes have degeneracy points with the other branches: 2 with 3 and 3 with 1, see Fig. 2.

Given the generic property of the eigenenergies mentioned after (S12) and that one of the magnon modes is flat, it follows that $\varepsilon_{2, \mathbf{k}} + \varepsilon_{3, \mathbf{k}} = \varepsilon_1$.

Dzyaloshinskii-Moria interaction

The Dzyaloshinskii-Moriya (DM) interaction is

$$\delta\hat{\mathcal{H}}_{DM} = \sum_{\langle ij \rangle} \mathbf{D}_{ij} \cdot (\mathbf{S}_i \times \mathbf{S}_j). \quad (\text{S16})$$

The most prevalent direction of the Dzyaloshinskii-Moria vector for the kagomé lattice is out of plane [2, 3]. To determine the choice of the DM vectors \mathbf{D}_{ij} one has to

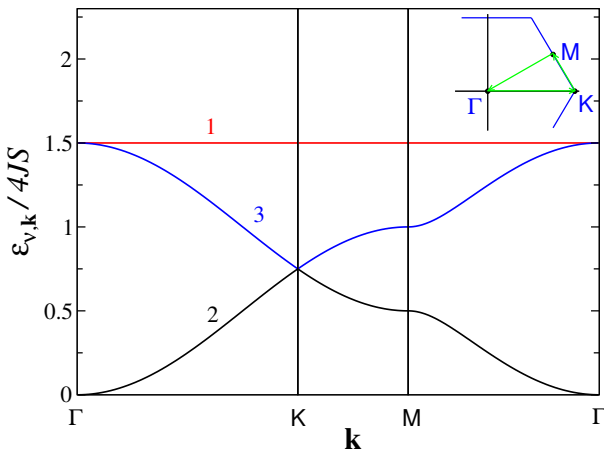


FIG. 2: Harmonic magnon energies for $\mathbf{M} \perp \mathbf{D}_{ij}$, which are equivalent to the $D = 0$ case (S15) and (S12).

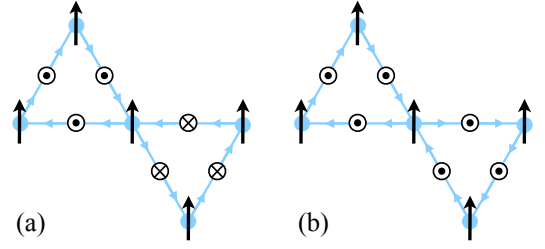


FIG. 3: Directions of the out-of-plane DM vectors. Arrows on the bonds show the ordering of the \mathbf{S}_i and \mathbf{S}_j operators in the vector-product in (S16).

specify the order of sites i and j in the vector product. One choice is given in Figure 3(a), in which the ordering of spins alternates from clockwise to counterclockwise between up and down triangles, leading to a uniform ordering along the chain directions. A choice in Figure 3(b) corresponds to a uniform (clockwise) ordering of spins in both up and down triangles and also to a uniform ordering around hexagons. The respective choices of the DM vectors are alternating in (a) and uniform in (b). These gauges are identical in their physical results.

There are two principal orientations of the magnetization \mathbf{M} of the ferromagnet to consider, the in-plane and the out-of-plane. It is clear, particularly from Figure 3(b), that the mean-field “tug” of the DM interactions on a spin from its neighbors vanishes identically due to its cancellation from different directions. That is, the contribution to the classical energy from, say, $\{1, 3\}$ bond cancels the one from the $\{1, 2\}$ bond.

Out-of-plane $\mathbf{M} \parallel \mathbf{D}_{ij}$

For magnetization $\mathbf{M} \parallel \mathbf{D}_{ij}$, spin quantization axis is $\hat{\mathbf{z}} \parallel \mathbf{M}$ with x - and y -axes within the kagomé plane. This corresponds to the DM vector $\mathbf{D}_{ij} = (0, 0, D)$ for the gauge of Fig. 3(b). Consider the DM term on $\{1, 2\}$ bond

$$\delta\hat{\mathcal{H}}_{DM}^{\{1,2\}} = -D(S_1^x S_2^y - S_1^y S_2^x). \quad (\text{S17})$$

There is no contribution to the classical energy, but the DM term contributes to the harmonic, quartic, etc., parts of the Hamiltonian. The harmonic part is

$$\delta\hat{\mathcal{H}}_{DM}^{(2)} = iDS \sum_{\ell} \left[a_{1, \ell}^{\dagger} (a_{2, \ell} + a_{2, \ell-3}) - a_{1, \ell}^{\dagger} (a_{3, \ell} + a_{3, \ell+1}) + a_{2, \ell}^{\dagger} (a_{3, \ell} + a_{3, \ell+2}) - \text{H.c.} \right], \quad (\text{S18})$$

in which one can see that the anomalous terms are not generated. After the Fourier transform (S6), it reads

$$\delta\hat{\mathcal{H}}_{DM}^{(2)} = 2DS \sum_{\mathbf{k}, \alpha\beta} \delta\Lambda_{\mathbf{k}}^{\alpha\beta} a_{\alpha, \mathbf{k}}^{\dagger} a_{\beta, \mathbf{k}}, \quad (\text{S19})$$

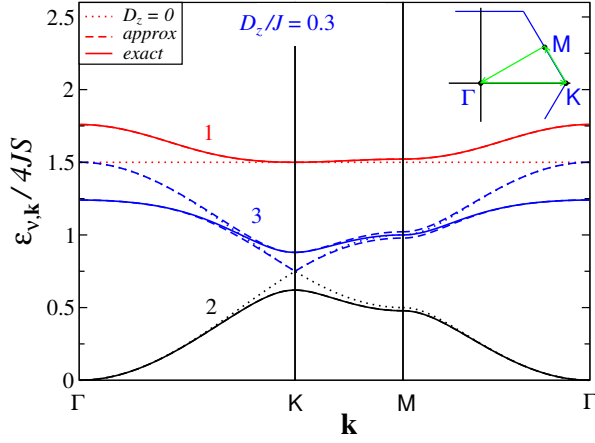


FIG. 4: Magnon energies for $D = 0.3J$. Solid lines are from exact solutions of (S23), dotted are the $D = 0$ results. Dashed lines (indistinguishable from solid lines for modes 1 and 2) are from approximate results (S25).

where we introduced the matrix

$$\delta \hat{\mathbf{A}}_{\mathbf{k}} = \begin{pmatrix} 0 & ic_3 & -ic_1 \\ -ic_3 & 0 & ic_2 \\ ic_1 & -ic_2 & 0 \end{pmatrix}. \quad (\text{S20})$$

Thus, the full harmonic Hamiltonian (S7)+(S19) can be written in the matrix form (S11) with $\hat{\mathbf{A}}_{\mathbf{k}} \Rightarrow \tilde{\mathbf{A}}_{\mathbf{k}}$ where

$$\tilde{\mathbf{A}}_{\mathbf{k}} = \hat{\mathbf{I}} - \frac{1}{2} \tilde{\mathbf{A}}_{\mathbf{k}}, \quad (\text{S21})$$

and the new matrix

$$\tilde{\mathbf{A}}_{\mathbf{k}} = \begin{pmatrix} 0 & (1-id)c_3 & (1+id)c_1 \\ (1+id)c_3 & 0 & (1-id)c_2 \\ (1-id)c_1 & (1+id)c_2 & 0 \end{pmatrix}, \quad (\text{S22})$$

where $d = D/J$. As in the pure Heisenberg case, the off-diagonal terms of the $\hat{\mathbf{H}}_{\mathbf{k}}$ matrix are zero and the eigenvalues of $\hat{\mathbf{H}}_{\mathbf{k}}$ and $\tilde{\mathbf{A}}_{\mathbf{k}}$ are straightforwardly related to the eigenvalues of the matrix $\tilde{\mathbf{A}}_{\mathbf{k}}$. The characteristic equation for the latter is

$$(\lambda + 1)(\lambda^2 - \lambda - 2\gamma_{\mathbf{k}}) = d^2(2\gamma_{\mathbf{k}}(\lambda - 3) + \lambda), \quad (\text{S23})$$

which is not solvable in a compact form anymore [4]. The resultant spin-wave energies are

$$\tilde{\varepsilon}_{\nu,\mathbf{k}} = 4JS\tilde{\omega}_{\nu,\mathbf{k}}, \quad \tilde{\omega}_{\nu,\mathbf{k}} = 1 - \tilde{\lambda}_{\nu,\mathbf{k}}/2. \quad (\text{S24})$$

Notably, the condition $\sum_{\nu} \varepsilon_{\nu,\mathbf{k}} = \text{const}$ persists.

Approximate solution.—For practical purposes, one may be interested in approximate solutions of the characteristic equation (S23), which are valid close to the degeneracy points of the Heisenberg-only spectrum. After some algebra, one can find an exceedingly accurate analytical solution for modes 1 and 2 (flat and Goldstone),

and two different solution for the mode 3 (gapped), becoming exact near each of the two degeneracy points

$$\begin{aligned} \tilde{\lambda}_{1(3),\mathbf{k}} &= \frac{\lambda_{1,\mathbf{k}}^{(0)} + \lambda_{3,\mathbf{k}}^{(0)}}{2} \pm \sqrt{\frac{(\lambda_{1,\mathbf{k}}^{(0)} - \lambda_{3,\mathbf{k}}^{(0)})^2}{4} + A_{1,\mathbf{k}}}, \\ \tilde{\lambda}_{2(3),\mathbf{k}} &= \frac{\lambda_{2,\mathbf{k}}^{(0)} + \lambda_{3,\mathbf{k}}^{(0)}}{2} \pm \sqrt{\frac{(\lambda_{2,\mathbf{k}}^{(0)} - \lambda_{3,\mathbf{k}}^{(0)})^2}{4} + A_{2,\mathbf{k}}}, \end{aligned} \quad (\text{S25})$$

where $\lambda_{\nu,\mathbf{k}}^{(0)}$ are solutions of the $D = 0$ problem (S14) and

$$\begin{aligned} A_{1,\mathbf{k}} &= d^2 \left(2\gamma_{\mathbf{k}}(\lambda_{1,\mathbf{k}}^{(0)} - 3) + \lambda_{1,\mathbf{k}}^{(0)} \right) / (\lambda_{1,\mathbf{k}}^{(0)} - \lambda_{2,\mathbf{k}}^{(0)}), \\ A_{2,\mathbf{k}} &= d^2 \left(2\gamma_{\mathbf{k}}(\lambda_{2,\mathbf{k}}^{(0)} - 3) + \lambda_{2,\mathbf{k}}^{(0)} \right) / (\lambda_{2,\mathbf{k}}^{(0)} - \lambda_{1,\mathbf{k}}^{(0)}). \end{aligned} \quad (\text{S26})$$

Figure 4 shows magnon energies for a representative $D = 0.3J$. The gaps at the Γ and K points are

$$\frac{\Delta_{\Gamma}}{4JS} = \sqrt{3}|d|, \quad \frac{\Delta_K}{4JS} = \frac{\sqrt{3}}{2}|d|, \quad (\text{S27})$$

respectively.

In-plane $\mathbf{M} \perp \mathbf{D}_{ij}$

For the in-plane $\mathbf{M} \perp \mathbf{D}_{ij}$ with $\hat{\mathbf{z}} \parallel \mathbf{M}$ and x -axis in the kagomé plane, $\mathbf{D}_{ij} = (0, -D, 0)$ in the gauge of Fig. 3(b). The DM term on the $\{1, 2\}$ bond becomes

$$\delta \hat{\mathcal{H}}_{DM}^{\{1,2\}} = D(S_1^z S_2^x - S_1^x S_2^z). \quad (\text{S28})$$

It is clear that this term gives zero contribution to the classical, harmonic, and other “even” terms of the bosonic $1/S$ expansion and only contributes to the “odd” ones. The terms linear in bosonic operators cancel, and the first non-zero contribution is cubic. Moreover, since the harmonic Hamiltonian, which in this case is provided only by the Heisenberg part (S7), is free from the off-diagonal terms, there are no quantum fluctuations in the ground state of the system. This, in turn, restricts the bosonic output of the DM term to the “decay” terms only, $b^\dagger b^\dagger b$, but *not* the “source” terms, $b^\dagger b^\dagger b^\dagger$. This is obvious because the unitary transformation that diagonalizes (S7) does not mix a operators with a^\dagger . Therefore, cubic terms cannot contribute to the ground-state energy. However, the decays of magnons are allowed.

A transparent real-space picture of these processes can be drawn for spin flips. The DM interaction (S28) creates (annihilates) a spin-flip in a proximity of another spin flip, see Fig. 5. Thus, one has a transition from a state with one magnon to a virtual one with two magnons. A second-order process involving this transition leads to the energy shift and correction to hopping, and, most importantly, to magnon decays.

Similarly to the cubic terms, the quartic terms, which are generated by the Heisenberg term (S1) and by the

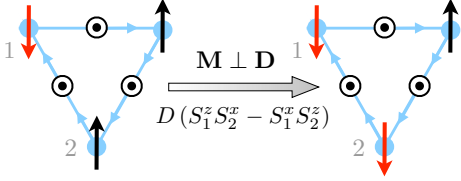


FIG. 5: Real-space process due to DM term in (S28).

DM term (S16) for $\mathbf{M} \not\perp \mathbf{D}$, necessarily have the form $a_i^\dagger a_j^\dagger a_j a_i$ or $a_i^\dagger a_i^\dagger a_i a_j$. Because of that, at $T=0$, the four-magnon and the other higher-order n -magnon terms do not affect the spectrum of the model directly.

Comment on the ground state—Formally, the situation is deceptively similar to the easy-plane antiferromagnet, as the DM-term is expected to act similarly to the easy-plane anisotropy. In the latter case, the anomalous terms *do occur* and there are fluctuations in the ground state, i.e. $|\mathbf{M}| < SN$. However, due to frustration between the DM terms on neighboring links, magnetization is fully saturated in the present case, regardless of the $\mathbf{M} - \mathbf{D}$ orientation. This can be rephrased as the following. If we prepare a fully saturated state along some axis with \mathbf{D} out-of-plane, the J -term and the \mathbf{M}_z -DM term (S17) cannot change the prepared state. For the \mathbf{M}_\perp -DM term (S28), the in-plane projections of each S_i^z are identical and the DM contribution to the ground state vanishes exactly due to cancellation from neighboring bonds. Thus, the DM term cannot generate fluctuations away from the fully saturated ground state. One can see immediately that this is not true for the excited states, as the local S_i^z are not identical for them. Therefore, the ground state is protected from the DM-induced quantum fluctuations while the spectrum is not.

Cubic terms for the in-plane $\mathbf{M} \perp \mathbf{D}_{ij}$ configuration

Consider $\mathbf{M} \perp \mathbf{D}_{ij}$. Some algebra yields the cubic terms from the DM interaction (S28)

$$\hat{\mathcal{H}}_{DM}^{(3)} = D \sqrt{\frac{2S}{N}} \sum_{\alpha\beta, \mathbf{k}, \mathbf{q}} \epsilon^{\alpha\beta\gamma} \cos(q\beta\alpha) a_{\alpha, \mathbf{q}}^\dagger a_{\beta, \mathbf{k}}^\dagger a_{\beta, \mathbf{P}} + \text{H.c.}, \quad (\text{S29})$$

with the structure which is virtually identical to the one in the kagomé-lattice antiferromagnet in the $\mathbf{q}=0$ phase [1], where $\mathbf{p} = \mathbf{k} + \mathbf{q}$, $q\beta\alpha = \mathbf{q}\boldsymbol{\rho}\beta\alpha$ with $\boldsymbol{\rho}\beta\alpha = \boldsymbol{\rho}\beta - \boldsymbol{\rho}\alpha$, and $\epsilon^{\alpha\beta\gamma}$ is the Levi-Civita antisymmetric tensor.

The unitary transformation that diagonalizes Hamiltonian in (S11) can always be written as [1]

$$b_{\nu, \mathbf{k}} = \sum_{\alpha} w_{\nu, \alpha}(\mathbf{k}) a_{\alpha, \mathbf{k}}, \quad a_{\alpha, \mathbf{k}} = \sum_{\nu} w_{\nu, \alpha}(\mathbf{k}) b_{\nu, \mathbf{k}}, \quad (\text{S30})$$

where the eigenvectors $\mathbf{w}_\nu = (w_{\nu, 1}, w_{\nu, 2}, w_{\nu, 3})$

$$\hat{\Lambda}_{\mathbf{k}} \mathbf{w}_\nu = \lambda_{\nu, \mathbf{k}} \mathbf{w}_\nu \quad (\text{S31})$$

can be written explicitly for $\mathbf{M} \perp \mathbf{D}_{ij}$ as

$$\mathbf{w}_\nu = \frac{1}{r_\nu} \begin{pmatrix} c_1 c_2 + \lambda_\nu c_3 \\ \lambda_\nu^2 - c_1^2 \\ c_1 c_3 + \lambda_\nu c_2 \end{pmatrix}, \quad (\text{S32})$$

and $r_\nu = \sqrt{(c_1 c_2 + \lambda_\nu c_3)^2 + (\lambda_\nu^2 - c_1^2)^2 + (c_1 c_3 + \lambda_\nu c_2)^2}$.

We emphasize that this analytic expression for the eigenvectors is only valid for $\mathbf{M} \perp \mathbf{D}$, because the linear spin-wave Hamiltonian does not have any contributions from the DM-terms in this case. For the tilted $\mathbf{M} - \mathbf{D}$ configuration, considered later, the *form* of the transformation in (S30) and the corresponding structure of expressions for the cubic vertex below (S33) are the same, but the matrix to diagonalize is $\hat{\mathbf{A}}_{\mathbf{k}}$ from (S23) with $d \rightarrow d \cos \theta$. This diagonalization can be done numerically [4].

Applying unitary transformation of (S30) to (S29) with the subsequent symmetrization yields

$$\hat{\mathcal{H}}_{DM}^{(3)} = \frac{1}{2!} \sqrt{\frac{1}{N}} \sum_{\mathbf{k}, \mathbf{q}} \sum_{\nu\mu\eta} \Phi_{\mathbf{q}\mathbf{k}; \mathbf{p}}^{\nu\mu\eta} b_{\nu, \mathbf{q}}^\dagger b_{\mu, \mathbf{k}}^\dagger b_{\eta, \mathbf{p}} + \text{H.c.}, \quad (\text{S33})$$

with the vertex

$$\Phi_{\mathbf{q}\mathbf{k}; \mathbf{p}}^{\nu\mu\eta} = D\sqrt{2S} \tilde{\Phi}_{\mathbf{q}\mathbf{k}; \mathbf{p}}^{\nu\mu\eta} = D\sqrt{2S} \left(F_{\mathbf{q}\mathbf{k}\mathbf{p}}^{\nu\mu\eta} + F_{\mathbf{k}\mathbf{q}\mathbf{p}}^{\mu\nu\eta} \right), \quad (\text{S34})$$

and the amplitude

$$F_{\mathbf{q}\mathbf{k}\mathbf{p}}^{\nu\mu\eta} = \sum_{\alpha\beta} \epsilon^{\alpha\beta\gamma} \cos(q\beta\alpha) w_{\nu, \alpha}(\mathbf{q}) w_{\mu, \beta}(\mathbf{k}) w_{\eta, \beta}(\mathbf{p}). \quad (\text{S35})$$

Using the dimensionless vertex (S34) and frequencies (S12) one can write the on-shell, $\omega = \varepsilon_{\mu, \mathbf{k}}$, relaxation rate as

$$\Gamma_{\mu, \mathbf{k}} = \frac{\pi J d^2}{4N} \sum_{\mathbf{q}, \nu\eta} \left| \tilde{\Phi}_{\mathbf{q}, \mathbf{k}-\mathbf{q}; \mathbf{k}}^{\nu\eta\mu} \right|^2 \delta(\omega_{\mu, \mathbf{k}} - \omega_{\nu, \mathbf{q}} - \omega_{\eta, \mathbf{k}-\mathbf{q}}), \quad (\text{S36})$$

and the $1/S$ correction to the spectrum

$$\text{Re}\Sigma_{\mu, \mathbf{k}} = \frac{J d^2}{4N} \sum_{\mathbf{q}, \nu\eta} \frac{\left| \tilde{\Phi}_{\mathbf{q}, \mathbf{k}-\mathbf{q}; \mathbf{k}}^{\nu\eta\mu} \right|^2}{\omega_{\mu, \mathbf{k}} - \omega_{\nu, \mathbf{q}} - \omega_{\eta, \mathbf{k}-\mathbf{q}}}, \quad (\text{S37})$$

where we made explicit that they are $\propto d^2$ and thus, naively, should not be significant for most real materials.

Note on the self-energy.—We point out that the magnon self-energies in (S36), (S37) and in the subsequent consideration are the *diagonal* elements of the 3×3 matrix. Nevertheless, in the Born approximation, contributions of the off-diagonal elements to the main poles in the spectrum are of significantly higher order, $O(d^4)$, and can be safely neglected. The only possibly dangerous region concerns the vicinity of $\mathbf{k} = 0$ point where modes 1 and 3 are in a resonance-like condition. However, at this point the $1 \leftrightarrow \{2, 3\}$ and $3 \leftrightarrow \{2, 3\}$ coupling vertices $\tilde{\Phi}_{\mathbf{q}, \mathbf{k}-\mathbf{q}; \mathbf{k}}^{233}$ and $\tilde{\Phi}_{\mathbf{q}, \mathbf{k}-\mathbf{q}; \mathbf{k}}^{231}$ are orthogonal, yielding a vanishing off-diagonal $\Sigma_{13, \mathbf{k}=0}$. In the following, we, therefore, neglect the off-diagonal self-energies entirely.

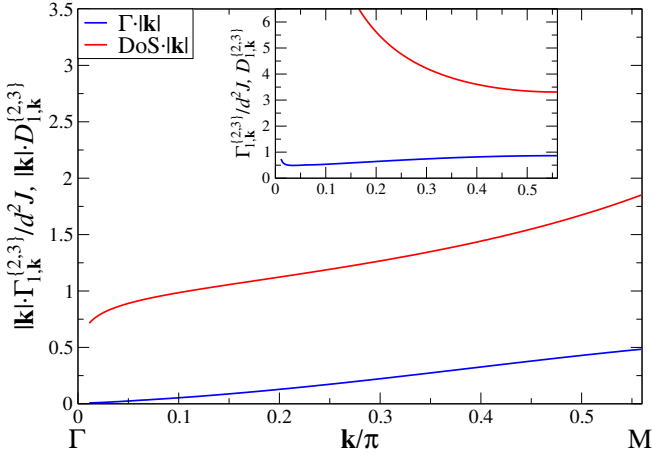


FIG. 6: The relaxation rate $\Gamma_{1,\mathbf{k}}^{\{2,3\}}$ and the two-magnon DoS $D_{1,\mathbf{k}}^{\{2,3\}}$ (times $|\mathbf{k}|$) along the ΓM line. The unphysical up(down)turns near $|\mathbf{k}| = 0$ are due to finite-size effect in the numerical integration. Inset: $\Gamma_{1,\mathbf{k}}^{\{2,3\}}$ and $D_{1,\mathbf{k}}^{\{2,3\}}$.

Decays and divergences for $\mathbf{M} \perp \mathbf{D}_{ij}$

Analysis of the energy and momentum conservation in the decay process, $\omega_{\mu,\mathbf{k}} \rightarrow \omega_{\nu,\mathbf{q}} + \omega_{\eta,\mathbf{k}-\mathbf{q}}$, for the bands in Fig. 2 suggests that the only possible decay channels are flat into a mix of Goldstone and gapped, $1 \rightarrow \{2,3\}$, Goldstone into itself, $2 \rightarrow \{2,2\}$, and gapped into two Goldstones or a mix of gapped and Goldstone, $3 \rightarrow \{2,2\}$ and $3 \rightarrow \{2,3\}$. The LSW dispersions of the magnon bands in the case $\mathbf{M} \perp \mathbf{D}$ in Fig. 2 correspond to $D=0$, because the DM-term does not contribute to the harmonic theory.

The decay channels $2(3) \rightarrow \{2,2\}$ are “regular” and yield the decay rates of the corresponding modes that are $\propto d^2$ and are only noticeable near the edge of the Brillouin zone for kinematic reasons, as can be verified numerically. The situation with the $1(3) \rightarrow \{2,3\}$ decays is different. From the kinematic perspective, the $\mathbf{k} = 0$ point for both modes is massively degenerate because the decay condition, $\omega_{1(3),\mathbf{k}=0} = \omega_{2,\mathbf{q}} + \omega_{3,-\mathbf{q}}$, is satisfied for *any* value of \mathbf{q} of the decay products. This is the consequence of the property of the spectrum $\sum_{\nu} \varepsilon_{\nu,\mathbf{k}} = \text{const}$ discussed above.

Two-magnon density-of-states (DoS) for the $1(3) \rightarrow \{2,3\}$ channels is given by

$$D_{1(3),\mathbf{k}}^{\{2,3\}} = \pi \sum_{\mathbf{q}} \delta(\omega_{1(3),\mathbf{k}} - \omega_{2,\mathbf{q}} - \omega_{3,\mathbf{k}-\mathbf{q}}). \quad (\text{S38})$$

As is shown in Figs. 6 and 7, the two-magnon DoS in the $1(3) \rightarrow \{2,3\}$ channels diverges as $1/|\mathbf{k}|$ at $\mathbf{k} \rightarrow 0$ as a consequence of the degeneracy discussed above. One can also verify this divergence analytically using small-momentum expansion for magnon energies.

Same Figures show the corresponding $\Gamma_{1(3),\mathbf{k}}$ from (S36). While the on-shell broadening for mode 3, $\Gamma_{3,\mathbf{k}}$,

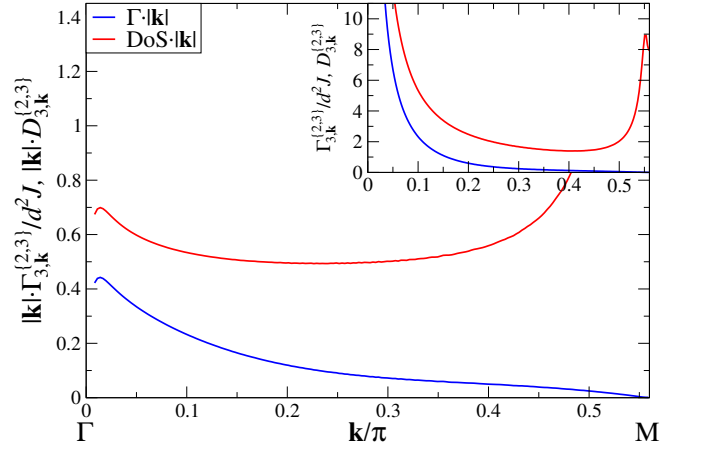


FIG. 7: Same as in Fig. 6 for $\Gamma_{3,\mathbf{k}}^{\{2,3\}}$ and $D_{3,\mathbf{k}}^{\{2,3\}}$.

clearly follows the divergence in DoS, the expected $1/|\mathbf{k}|$ -divergence for the flat mode is preempted by a subtle cancellation in the decay vertex, leading to a constant $\Gamma_{1,\mathbf{k}} (\propto d^2)$ at $\mathbf{k} \rightarrow 0$.

The on-shell corrections to the magnon energies $\text{Re}\Sigma_{\mu,\mathbf{k}}$ in (S37) also contain $\mathbf{k} \rightarrow 0$ divergences. In general, all six self-energy terms from the channels $1(3) \rightarrow \{\nu,\eta\}$ contribute. Four of them are regular ($\propto d^2$) and two yield logarithmic divergences, see Fig. 8. In addition to the channels $1(3) \rightarrow \{2,3\}$, the $1(3) \rightarrow \{1,2\}$ channels, which do not contribute to the decays, also contribute to the divergences in $\text{Re}\Sigma_{\mu,\mathbf{k}}$. A small-momentum expansion can confirm, after some algebra, the $\ln|\mathbf{k}|$ -character of the divergences. Interestingly, while the on-shell $\Gamma_{1,\mathbf{k}}$ is not divergent, the real part of the self-energy shows the same $\ln|\mathbf{k}|$ -divergence as for the mode 3. Although the logarithmic divergence is much weaker than $1/|\mathbf{k}|$ in $\Gamma_{\mathbf{k}}$, it has similar roots and requires a regularization.

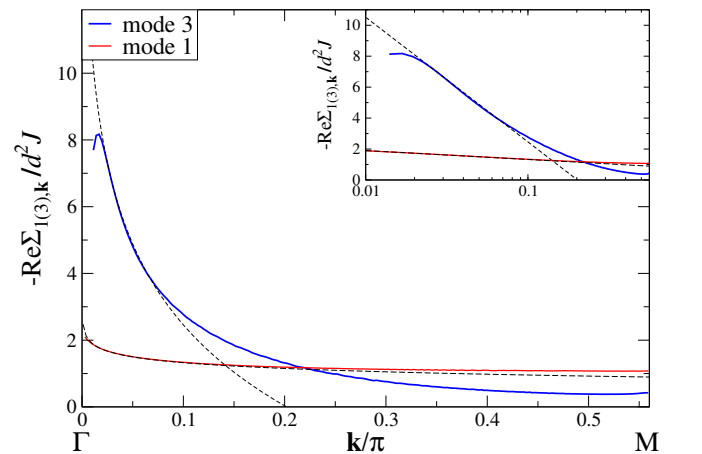


FIG. 8: Real part of the on-shell self-energies $\Sigma_{1(3),\mathbf{k}}^{\{2,3\}}$ along the ΓM line. Finite-size effects are also present at small \mathbf{k} , but can be identified by using more points in the numerical integration, which shifts the associated unphysical downturns to a smaller range of \mathbf{k} . Inset: same on the semi-log plot.

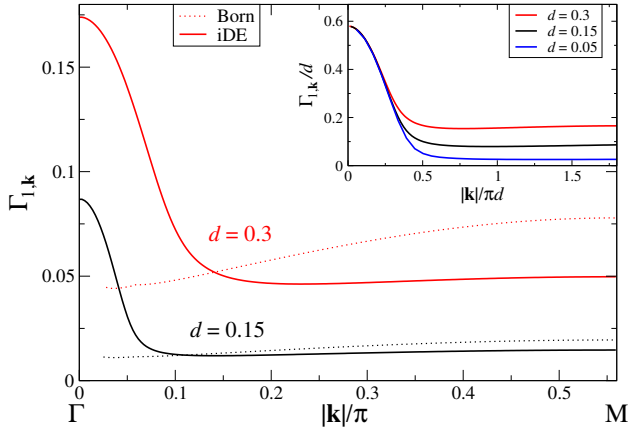


FIG. 9: $\Gamma_{1,\mathbf{k}}$ vs $|\mathbf{k}|$ from (S42) for $1 \rightarrow \{2, 3\}$ channel along the ΓM path for two representative $d = 0.3$ and $d = 0.15$ (solid lines). Dotted lines are Born approximation results (S36). Inset: $\Gamma_{1,\mathbf{k}}/d$ vs $|\mathbf{k}|/d$ for several values of d .

Regularization of divergences

A regularization can be achieved by a physical self-consistency requirement on damping of the initial-state magnon. Consider the Dyson's equation (DE) for a pole of the magnon Green's function of the branch μ

$$\omega - \varepsilon_{\mu,\mathbf{k}} - \Sigma_{\mu,\mathbf{k}}(\omega^*) = 0, \quad (\text{S39})$$

where $\Sigma_{\mu,\mathbf{k}}(\omega)$ is the decay self-energy due to cubic terms (S33). The complex conjugate $\omega^* = \bar{\varepsilon}_{\mu,\mathbf{k}} + i\Gamma_{\mu,\mathbf{k}}$ respects causality, see Ref. [5] for methodological and technical details. The real and imaginary parts of (S39) are

$$\begin{aligned} \bar{\varepsilon}_{\mu,\mathbf{k}} &= \varepsilon_{\mu,\mathbf{k}} + \text{Re} \Sigma_{\mu,\mathbf{k}}(\bar{\varepsilon}_{\mu,\mathbf{k}} + i\Gamma_{\mu,\mathbf{k}}), \\ \Gamma_{\mu,\mathbf{k}} &= -\text{Im} \Sigma_{\mu,\mathbf{k}}(\bar{\varepsilon}_{\mu,\mathbf{k}} + i\Gamma_{\mu,\mathbf{k}}), \end{aligned} \quad (\text{S40})$$

which have to be solved together. However, once the imaginary part is introduced, the logarithmic divergence in $\text{Re} \Sigma_{\mu,\mathbf{k}}$ is going to be cut [5]. Therefore, for small d , one can neglect the correction to the real part of the spectrum $\propto d^2 \ln d$. This approximation should be valid as long as the imaginary part obtained within the regularization is much larger, which is justified, as we show below, for realistic $d \lesssim 0.3$ because $\Gamma_{\mu,\mathbf{k}} \propto |d|$. With that, one arrives at the “imaginary-only” version of the Dyson's equation (iDE)

$$\Gamma_{\mu,\mathbf{k}} = -\text{Im} \Sigma_{\mu,\mathbf{k}}(\varepsilon_{\mu,\mathbf{k}} + i\Gamma_{\mu,\mathbf{k}}). \quad (\text{S41})$$

Thus, the self-consistent equation on damping is

$$1 = \frac{d^2}{16S} \sum_{\nu,\eta,\mathbf{q}} \frac{|\tilde{\Phi}_{\mathbf{q},\mathbf{k}-\mathbf{q};\mathbf{k}}^{\nu\eta\mu}|^2}{(\omega_{\mu,\mathbf{k}} - \omega_{\nu,\mathbf{q}} - \omega_{\eta,\mathbf{k}-\mathbf{q}})^2 + (\Gamma_{\mu,\mathbf{k}}/4JS)^2}, \quad (\text{S42})$$

where $\omega_{\nu,\mathbf{k}}$'s are the magnon frequencies in the linear spin-wave theory (S15). At small $|\mathbf{k}|$, the difference of the single- and two-magnon energies for the divergent

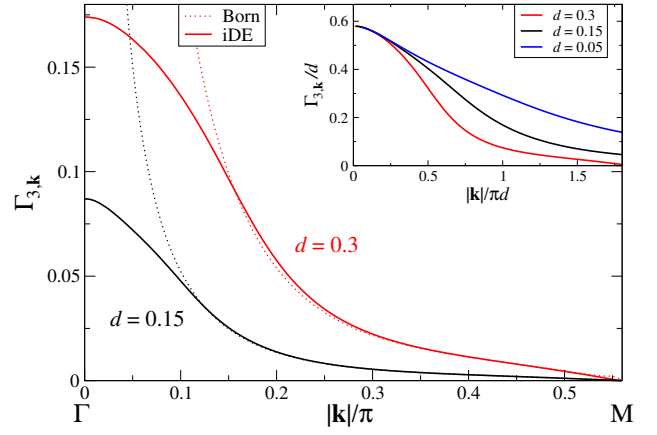


FIG. 10: Same as Fig. 9 for $\Gamma_{3,\mathbf{k}}$.

decay channels $\mu \rightarrow \{2, 3\}$ vanishes, contributing $O(|\mathbf{k}|^2)$ to the denominator of (S42), neglecting which yields

$$\Gamma_{\mu,\mathbf{k} \rightarrow 0} \approx J|d| \left(2S \sum_{\mathbf{q}} |\tilde{\Phi}_{\mathbf{q},\mathbf{k}-\mathbf{q};\mathbf{k}}^{23\mu}|^2 \right)^{1/2} \approx a_0 J|d| \sqrt{S}, \quad (\text{S43})$$

where $a_0 \approx 1$ is a constant. This is the main result of the iDE regularization. The decay rate of both flat and gapped modes at $\mathbf{k} \rightarrow 0$ is finite and is of the order of the *first* power of the DM coupling, $\Gamma_{1(3),\mathbf{k}} \propto |d|$. That is, it is strongly enhanced compared to a perturbative expectation and is nonanalytic. It is also much larger than the magnon energy shift, in agreement with the assumption made above. This vindicates the validity of the proposed iDE regularization scheme and also justifies the on-shell nature of our calculations. The \mathbf{k} -region in which the broadening is strongly enhanced is $|\mathbf{k}| \lesssim |\mathbf{k}^*| \propto d$ with the damping decreasing to the perturbative values $\Gamma_{3(1),\mathbf{k}} \propto d^2$ for $|\mathbf{k}| \gtrsim |\mathbf{k}^*|$.

One additional feature that follows from the not so obvious symmetry between $\tilde{\Phi}_{\mathbf{q},\mathbf{k}-\mathbf{q};\mathbf{k}}^{233}$ and $\tilde{\Phi}_{\mathbf{q},\mathbf{k}-\mathbf{q};\mathbf{k}}^{231}$ vertices at $\mathbf{k} \rightarrow 0$, is that the decay rates of the gapped and flat modes are equal at $\mathbf{k} = 0$. While a finite decay rate for the gapped mode is the result of the regularization, the decay rate of the flat mode is, somewhat surprisingly, *enhanced* from the perturbative value. However, the avoided divergence in the perturbative decay rate of the flat mode can be seen as a result of a fine tuning. As a result of the self-consistently introduced “fuzziness” of the decaying magnon, the strict conditions on the energy and momenta in the decay process are removed and allow the avoided divergence in the two-magnon density of states to surface up and be regularized the same way as for the gapped mode.

To demonstrate these trends, the numerical solutions of a simplified version of (S42) that includes only the divergent decay channels, $\{\nu, \eta\} = \{2, 3\}$, are shown in Figs. 9 and 10 for the flat and gapped modes, respectively, along the ΓM path. Born approximation results are also shown for comparison. In agreement with

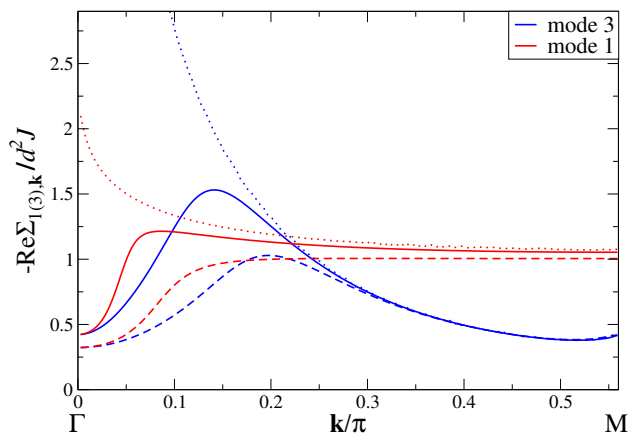


FIG. 11: Real part of the self-energies $\Sigma_{1(3),\mathbf{k}}^{\{2,3\}}$ (in units of Jd^2) along the ΓM line with $\Gamma_{1(3),\mathbf{k}}$ from Eq. (S42) for $d = 0.15$ (solid) and $d = 0.3$ (dashed). Born approximation results (S37) are shown by the dotted lines.

the qualitative discussion above, the characteristic region in $|\mathbf{k}|$ where damping is enhanced is of the order of d , although it has a strong subleading correction for the gapped mode, likely due to more conventional van Hove singularities in the two-magnon continuum [6]. Numerically, it is also a factor of 2 wider for the gapped mode than for the flat mode. While the decay rate $\Gamma_{3,\mathbf{k}}$ declines towards the edge of the Brillouin zone, the damping of the flat mode there is roughly a constant ($\propto d^2$).

Re Σ consistency.—In the iDE approach, $\text{Re}\Sigma$ was neglected. We verify a consistency of this assumption by evaluating $\text{Re}\Sigma_{\mu,\mathbf{k}}(\omega_{\mu,\mathbf{k}})$ in (S39) with the self-consistently determined $\Gamma_{\mu,\mathbf{k}}$ from (S42), see Fig. 11. The logarithmic divergence of the Born approximation is clearly regularized and magnon spectrum correction remains of order d^2 , and thus is negligible.

Note on the other channels.—In the iDE consideration above, only $1(3) \rightarrow \{2,3\}$ channels were used. According to the on-shell kinematic analysis, one should add the $3 \rightarrow \{2,2\}$ channel to make it complete. However, the “fuzziness” of the initial-state magnons opens up other channels that are not allowed in the Born approximation, such as $1(3) \rightarrow \{1,2\}$ and others. While they leave the qualitative results of the restricted iDE unchanged, they provide quantitative corrections and also modify the angular dependence of the damping of the flat mode, discussed next. In the following, in the iDE calculations using (S42) all channels are included.

$\mathbf{M} \angle \mathbf{D}_{ij}$ angular dependence

We have considered two principal orientations of the magnetization \mathbf{M} with respect to the out-of-plane DM vector, $\mathbf{M} \parallel \mathbf{D}_{ij}$ and $\mathbf{M} \perp \mathbf{D}_{ij}$. As is already well-known, in the former case magnon bands split with the gaps of the order of $O(d)$. Interaction among magnons

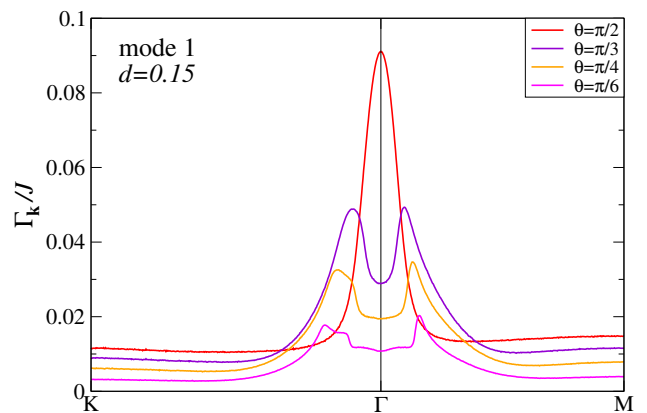


FIG. 12: Numerical results from (S42) for $\Gamma_{1,\mathbf{k}}$ for $d = 0.15$ along the K Γ M path for several θ .

does not contribute at $T = 0$ in this case, meaning that magnons are sharply-defined excitations. For the latter case, we demonstrated that the flat and gapped branches near the Γ point acquire an anomalous broadening, also $O(d)$. Given that the magnetization in the ideal model (S1)+(S16) is not pinned to any specific direction, and thus is easy to manipulate with an infinitesimal external magnetic field, the evolution from the decay-free excitations to the broadened excitations as a function of the angle between \mathbf{M} and \mathbf{D} is of interest.

For \mathbf{M} making an angle θ with the out-of-plane \mathbf{D} , there are three modifications of our considerations. First, the in-plane projection of magnetization is responsible for the cubic coupling (S28). This translates into the change in the corresponding vertices (S34), modifying the overall scale of the decay rates considered above by $d \Rightarrow d \sin \theta$ in their prefactors. Second, the out-of-plane component of magnetization is responsible for the complex hoppings of magnons (S19), thus modifying magnon spectra (S24) with gaps (S27) with the rescaling $d \Rightarrow d \cos \theta$. Lastly, due to the same complex hoppings, there is also a change in the eigenvectors $\mathbf{w}_\nu(\mathbf{k})$ in (S32), which enter the cu-

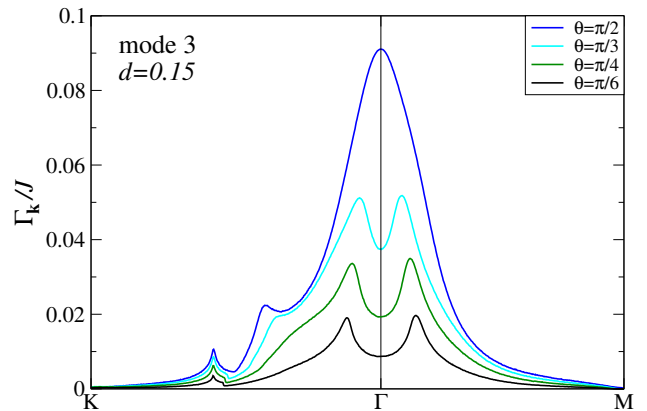


FIG. 13: Same as in Fig. 12 for $\Gamma_{3,\mathbf{k}}$.

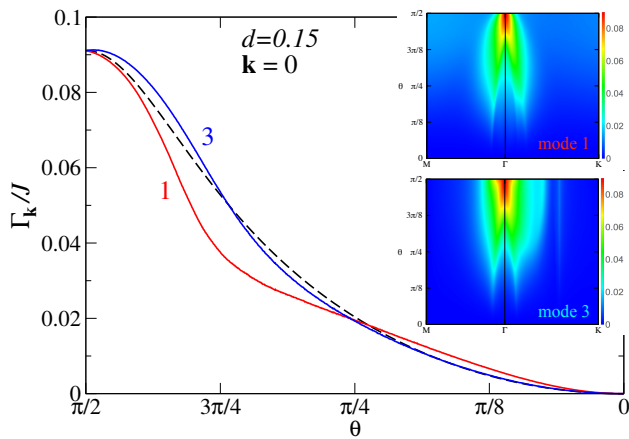


FIG. 14: $\Gamma_{1(3),\mathbf{k}}$ for $d = 0.15$ at $\mathbf{k} = 0$ vs the \mathbf{M} — \mathbf{D} angle θ . Dashed line is an interpolation, see the text. Inset: the 2D $\mathbf{k} - \theta$ intensity maps for both modes.

bic vertices (S34). These eigenvectors are not derivable analytically anymore in a compact form [4], and we obtain them numerically from diagonalization of the matrix in (S22). We note that in addition to the weakening of the magnon coupling ($\propto \sin \theta$), opening of the gaps ($\propto d \cos \theta$) reduces the degeneracy in the two-magnon continuum and provides a natural regularization.

We demonstrate the effects of the \mathbf{M} — \mathbf{D} orientation on the magnon damping by providing \mathbf{k} dependencies of $\Gamma_{\mathbf{k}}$ for $d = 0.15$ along a representative \mathbf{k} -path for both optical modes for several values of the angle θ in Figs. 12 and 13. All results are obtained by solving numerical iDE equation in (S42) with all possible channels. This picture is also accompanied by the angular dependence of the broadening of both modes at $\mathbf{k} = 0$ in Fig. 14, the behavior that can be checked experi-

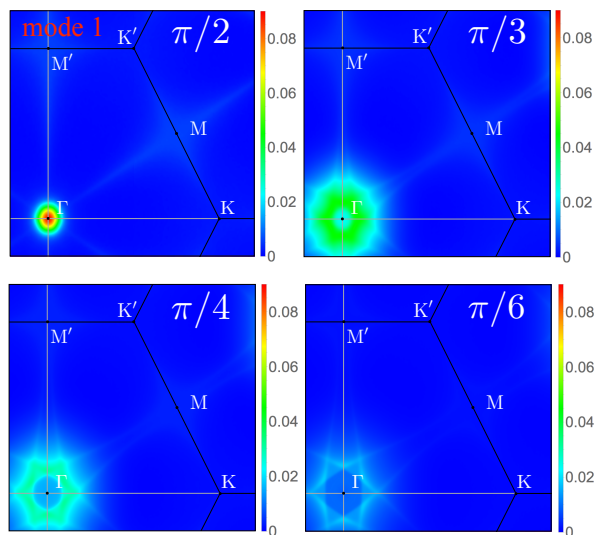


FIG. 15: $\Gamma_{1,\mathbf{k}}$ 2D \mathbf{k} intensity map for several representative θ for $d = 0.15$.

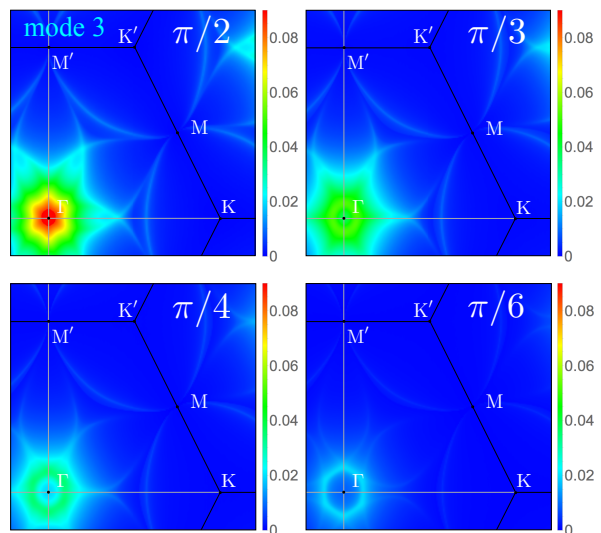


FIG. 16: Same as in Fig. 15 for $\Gamma_{3,\mathbf{k}}$.

mentally by ESR [7]. A simple interpolation formula: $\Gamma_0(\theta) = \Gamma_0(\pi/2)|\sin \theta|/\sqrt{1 + B \cot^2 \theta}$, for the choice of $B = 9.2$, agrees fairly well with the numerical iDE results, see Fig. 14. The same Figure also shows the detailed 2D $\mathbf{k} - \theta$ intensity maps of the broadenings along a representative \mathbf{k} -direction.

Our consideration is completed in Figs. 15 and 16 by the 2D \mathbf{k} -maps of $\Gamma_{\mathbf{k}}$ for several representative angles. In addition to the trends discussed previously, this comprehensive analysis reveals an interesting contribution of the other, conventional van Hove singularities in the two-magnon continuum [6] and suggests a rather unusual evolution of the magnon linewidth across the Brillouin zone.

We thus provided detailed predictions regarding the angular dependence of the damping of the optical magnon modes. The suggested dramatic picture can be tested by the neutron-scattering as well as the other techniques such as ESR or neutron-scattering spin-echo.

-
- [1] A. L. Chernyshev and M. E. Zhitomirsky, Phys. Rev. Lett. **113**, 237202 (2014); Phys. Rev. B **92**, 144415 (2015).
 - [2] M. Elhajal, B. Canals, and C. Lacroix, Phys. Rev. B **66**, 014422 (2002).
 - [3] O. Cepas, C. M. Fong, P. W. Leung, and C. Lhuillier, Phys. Rev. B **78**, 140405 (2008).
 - [4] See Supplemental Material of H. Katsura, N. Nagaosa, and P. A. Lee, Phys. Rev. Lett. **104**, 066403 (2010).
 - [5] A. L. Chernyshev and M. E. Zhitomirsky, Phys. Rev. B **79**, 144416 (2009).
 - [6] M. E. Zhitomirsky and A. L. Chernyshev, Rev. Mod. Phys. **85**, 219 (2013).
 - [7] R. Chisnell, J. S. Helton, D. E. Freedman, D. K. Singh, R. I. Bewley, D. G. Nocera, and Y. S. Lee, Phys. Rev. Lett. **115**, 147201 (2015).